World Journal of Innovative Research (WJIR)
ISSN: 2454-8236, Volume-5, Issue-2, August 2018 Pages 24-29

Pointing Bias in "Spatial Matched Filter" Beamforming at a Tri-Axial Velocity-Sensor due to Non-Perpendicular Axes

Chibuzo Joseph NNONYELU

***Abstract* -- This paper investigates how non-perpendicularity in a tri-axial velocity sensor would affect the tri-axial velocity-sensor's azimuth-elevation beam-pattern in terms of the beam's pointing direction and directivity. The vertical axis was adopted as the reference axis for the analysis and a rotation matrix developed to represent the non-perpendicularity in Euclidean space. The beampattern of this deformed tri-axial velocity sensor is then analytically studied. It was found that the non-perpendicularity does not affect the overall shape of the beampattern, but only introduces a pointing offset. Also, the non-perpendicularity imperfectionreduces the directivity of the imperfect triaxial velocity sensor relative to a perfect case. This finding developed in closed the pointing bias for the described deformity hence serves for non-iterative post data acquisition correction.**

***Index Terms* -- Spatial matched filter beamforming, tri-axial velocity sensor, pointing bias, array signal processing, vector sensors.**

I. INTRODUCTION

A. *A Tri-Axial Velocity-Sensor*

The ``tri-axial velocity sensor" (the "tri-axial velocity sensor" is also called a "velocity-sensor triad", a "pressure gradient sensor", an "acoustic vector-sensor", or a "vector hydrophone") measures an incident acoustic particle-velocity vector field by its three Cartesian spatial components. Such a "tri-axial velocity-sensor" has an array manifold of [1]–[3]

$$\mathbf{a}^{(3+0)}(\phi,\theta) = \begin{bmatrix} \cos\phi\sin\theta \\ \sin\phi\sin\theta \\ \cos\theta \end{bmatrix}, \quad (1)$$

where $\theta \in [0,\pi]$ denotes the polar arrival direction (also known as the zenith angle) defined with respect to the positive z-axis, and $\phi \in [0,2\pi)$ symbolizes the azimuth arrival direction defined with respect to the positive x-axis.

This "tri-axial velocity-sensor" has been implemented in hardware, sometimes with a collocating pressure-sensor.

The "tri-axial velocity-sensor" is available commercially, as the "Uniaxial P-U Probe" from AcousTech Inc. (Fort Wayne, Indiana, U.S.A.) for the underwater propagation medium, and as the "Ultimate Sound Probe" from Microflown Technologies (Arnhem, The Netherlands) and as "Vector Intensity Probe" from G.R.A.S. Sound and Vibration A/S (Holte, Denmark) for the air acoustics. The "tri-axial velocity-sensor"has been used in sea trials or aeroacoustic field tests, and has many signal-processing algorithms tailored for it --- please see [4]–[6] for comprehensive reviews of the research literature. The array manifold in (1) offers azimuth-elevation bivariate spatial directivity, plus independence from the frequency/spectrum/ bandwidth of the incident signal. This allows any associated signal processing to decouple the time/frequency coordinates from the direction-of-arrival coordinates. Furthermore, the spatial collocation of all three constituent sensors (i.e., the three *uni*-axial velocity-sensors) leads to a physical compactness that facilitates deployment and mobility.

B. *"Spatial Matched Filter" Beamforming on a Non-Orthogonal Tri-Axial Velocity-Sensor*

The array manifold in (1), however, implicitly presumes the tri-axial velocity-sensor's three axes to be perfectly perpendicular among themselves. Perfect orthogonality is an idealization unattainable in practical systems. What if they are not, perhaps due to manufacturing imperfections? Or, how much axial orthogonality exactness is required for the tri-axial velocity-sensor to function "properly", say, in "spatial matched filter" (SMF) beamforming?

"Spatial matched filter" (SMF) beamforming is common in data-independent beamforming, partly on account of its computational simplicity.It weights-and-sums the individual channels' measurements, by matching the beamforming weightsto the array's spatial-steering-vector weights toward a pre-set/fixed "look direction" of (ϕ_L,θ_L).If the interference and the additive noise together are statistically 1) zero in mean, 2) spatiallyuncorrelated, and 3) uncorrelated with the desired signal impinging from the pre-set "look direction" -- then this "spatial matched filter" beamformer's output signal-to-noise power ratio (SNR)would be would maximized[7].The tri-axial velocity-sensor's "spatial matched filter" beam-pattern has been analyzed in[8], [9]under the assumption of perfect orthogonality among the three axes.

For non-perpendicular axes, the "spatial match filter" beampattern has not been analyzed in the open literature (to the best knowledge of the present authors) for the *tri*-axial velocity-sensor.

The *bi*-axial velocity-sensor (i.e., the u-u probe) [10]has analytically proved to incur a directional pointing error, but the overall beam pattern would otherwise be same as in the perpendicular case.This paper will generalize the analysis in [10] to a *tri*-axial velocity-sensor, with the collocating pressure-sensor,under *tetra*-variate axial non-orthogonality.

Chibuzo Joseph NNONYELU, Electrical Engineering, University of Nigeria, Nsukka, Nigeria

C. Organization of This Paper

The preliminary analysis in SectionIIwill develop the rotation matrix that describes the non-perpendicular nature of the tri-axial velocity sensor under study.Section IIIwill analytically derive the pointing error in closed form, explicitly in terms of the tri-axial velocity-sensor's axial mis-orientation angles of $(\phi_x, \theta_x, \phi_y, \theta_y)$ and in terms ofthe beamformer's pre-set ``look direction'' (ϕ_L, θ_L).Section IVwill further analyze the pointing bias with z-axis as the reference axis, and insightful degenerate cases will also be studied.To study the effect of the pointing bias on the directivity of the sensor, SectionVwill analytically derive the directivity of the imperfect tri-axial velocity sensor.Section VIwill conclude this investigation.

II. The Geometry Of Axial Mis-Orientation

Without loss of generality, the z-axis is taken as the reference axis, i.e. the perfect axis. This section contains the rotations that would take x-, y- axes to $\tilde{x}$-, $\tilde{y}$- directions respectively.Figure 1 shows the how the nominal axes are rotated to the deformed axes.

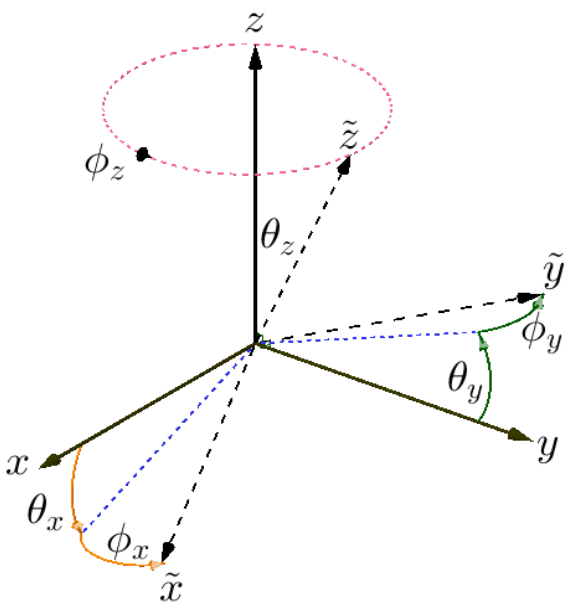

Figure 1. The tri-axial velocity-sensor, with *quad*-variate mis-orientation in its x-axis and y-axis. The four mis-orientation angles are (ϕ_x, θ_x) to parameterize the mis-orientation of the x-axis to the $\tilde{x}$-axis and (ϕ_y, θ_y) to parameterize the mis-orientation of the y-axis to the $\tilde{y}$-axis.

The rotation of a vector through an angle ψ about the x-, y-, or z-axis are captured in the basic rotation matrix

$$\mathbf{T}_x(\psi) = \begin{bmatrix} 1 & 0 & 0 \\ 0 & \cos\psi & -\sin\psi \\ 0 & \sin\psi & \cos\psi \end{bmatrix}, \quad (2)$$

$$\mathbf{T}_y(\psi) = \begin{bmatrix} \cos\psi & 0 & \sin\psi \\ 0 & 1 & 0 \\ -\sin\psi & 0 & \cos\psi \end{bmatrix}, \quad (3)$$

and

$$\mathbf{T}_z(\psi) = \begin{bmatrix} \cos\psi & -\sin\psi & 0 \\ \sin\psi & \cos\psi & 0 \\ 0 & 0 & 1 \end{bmatrix} \quad (4)$$

respectively.

To take x-axis to $\tilde{x}$-direction, the x-axis is mis-oriented to a new $\tilde{x}$-direction by $\mathbf{T}_{yz}(\theta_x, \phi_x)$ obtained by a rotation of

i. θ_x about the nominal y-axis captured in$\mathbf{T}_y(\theta_x)$and,
ii. ϕ_x about the nominal z-axis captured in $\mathrm{T}_z(\phi_x)$.

Therefore,

$$\mathbf{T}_{\mathrm{yz}}(\theta_x, \phi_x) = \mathbf{T}_z(\phi_x)\,\mathbf{T}_y(\theta_x) = \begin{bmatrix} \cos\phi_x\cos\theta_x & -\sin\phi_x & \cos\phi_x\sin\theta_x \\ \cos\theta_x\sin\phi_x & \cos\phi_x & \sin\phi_x\sin\theta_x \\ -\sin\theta_x & 0 & \cos\theta_x \end{bmatrix} \quad (5)$$

Applying similar steps for the rotation of the y-axis, the overall rotation matrix of the deformed tri-axial velocity sensor with z-axis as reference axis is given below

$$\mathbf{R}(\phi_x, \theta_x, \phi_y, \theta_y) = \begin{bmatrix} \cos\phi_x\cos\theta_x & \sin\phi_x\cos\theta_x & -\sin\theta_x \\ -\sin\phi_y\cos\theta_y & \cos\phi_y\cos\theta_y & \sin\theta_y \\ 0 & 0 & 1 \end{bmatrix}, \quad (6)$$

Hence, the array manifold of the deformed tri-axial velocity sensor is given as

$$\tilde{\mathbf{a}}^{(3+0)}(\phi, \theta, \phi_x, \theta_x, \phi_y, \theta_y) = \mathbf{R}(\phi_x, \theta_x, \phi_y, \theta_y)\,\mathbf{a}^{(3+0)}(\phi, \theta). \quad (7)$$

III. Toward An Analytical Derivation Of The Beamformer's Pointing Error

Suppose that "spatial matched filter" beamforming is performed on anon-orthogonal tri-axial velocity-sensor corresponding to that described in Section II,but without any awareness of that non-orthogonality.That is, the beamforming weight vector is spatially matched to (1), instead of to (7).Therefore, the beampattern equals

$$B^{(3+0)}(\phi, \theta, \phi_L, \theta_L, \phi_x, \theta_x, \phi_y, \theta_y) = \frac{\mathbf{a}^{(3+0)}(\phi_L, \theta_L)^T\,\mathbf{R}(\phi_x, \theta_x, \phi_y, \theta_y)\,\mathbf{a}^{(3+0)}(\phi, \theta)}{\max_{\phi,\theta}\left[\mathbf{a}^{(3+0)}(\phi_L, \theta_L)^T\,\mathbf{R}(\phi_x, \theta_x, \phi_y, \theta_y)\,\mathbf{a}^{(3+0)}(\phi, \theta)\right]}, \quad (8)$$

where$\phi_L \in [0, 2\pi)$ and $\theta_L \in [0, \pi]$ denote the beamformer's look azimuth angle and the look polar angle, respectively.

Applying the condition for equality in Cauchy-Schwarz inequality, the denominator in (8) may be re-written as$\left|\left|\mathbf{R}(\phi_x, \theta_x, \phi_y, \theta_y)^{\mathrm{T}}\,\mathbf{a}^{(3+0)}(\phi_L, \theta_L)\right|\right|$. For the mathematical justification, please refer to Proposition 1 in [10]. Consequentially,

$$B^{(3+0)}(\phi,\theta,\phi_L,\theta_L,\phi_x,\theta_x,\phi_y,\theta_y) = \frac{\overbrace{\left(\mathbf{R}(\phi_x,\theta_x,\phi_y,\theta_y)^T\,\mathbf{a}^{(3+0)}(\phi_L,\theta_L)\right)^T}^{\mathbf{u}:=}}{\left\|\mathbf{R}(\phi_x,\theta_x,\phi_y,\theta_y)^T\,\mathbf{a}^{(3+0)}(\phi_L,\theta_L)\right\|}\,\mathbf{a}^{(3+0)}(\phi,\theta). \quad (9)$$

The fraction in (9) is a unit-vector; any unit-vector may be mathematicallyrepresented as a point on a unit-radius sphere that is centered upon the Cartesian origin.Any such point on the unit-sphere's surface is uniquely identified by an azimuth angle of ϕ_B and a polar angle ofθ_B.These two angles may be defined with reference to any point on the unit-sphere, say, with reference to (ϕ_L,θ_L), the beamformer's ``look direction''. In other words, $\boldsymbol{u}$ may be expressed as the 3×1 vector,

$$\begin{aligned}\mathbf{u} &:= \begin{bmatrix}\cos(\phi_L-\phi_B)\ \sin(\theta_L-\theta_B)\\ \sin(\phi_L-\phi_B)\ \sin(\theta_L-\theta_B)\\ \cos(\theta_L-\theta_B)\end{bmatrix},\\ &= \mathbf{a}^{(3+0)}(\phi_L-\phi_B,\theta_L-\theta_B).\end{aligned} \quad (10)$$

Therefore, the non-orthogonal tri-axial velocity-sensor'sSMF beam-pattern is same as that of the orthogonal case, except a bias of ϕ_B imposed on the look azimuth angle of $\phi_L$and a bias of θ_B imposed on the look polar angle of θ_L.

$$\begin{aligned}&B^{(3+0)}(\phi,\theta,\phi_L,\theta_L,\phi_x,\theta_x,\phi_y,\theta_y) =\\ &B^{(3+0)}(\phi,\theta,\phi_L-\phi_B,\theta_L-\theta_B,0,0,0,0).\end{aligned} \quad (11)$$

In the above,

$$\phi_B = \phi_L - \tan^{-1}\left(\frac{[\mathbf{u}]_2}{[\mathbf{u}]_1}\right) \quad (12)$$

$$\theta_B = \theta_L - \cos^{-1}[\mathbf{u}]_3, \quad (13)$$

where $[\mathbf{u}]_i$ denotes the ith entry of the vector $\mathbf{u}$.

The true direction of the beampattern's peak i.e.$\phi_{\text{peak}} = \phi_L - \phi_B$ and$\theta_{\text{peak}} = \theta_L - \theta_B$are stated as

$$\phi_{\text{peak}} = \tan^{-1}\left(\frac{[\mathbf{u}]_2}{[\mathbf{u}]_1}\right) \quad (14)$$

$$\theta_{\text{peak}} = \cos^{-1}[\mathbf{u}]_3 \quad (15)$$

Other than the above shift (ϕ_B,θ_B) imposed on the nominal look direction (ϕ_L,θ_L), the beampattern shape remains unchanged. That is, no additional side lobes or increase in the beamwidth.

The pointing bias (12) and (13) are expanded as

$$\phi_B = \phi_L - \tan^{-1}\left(\frac{\sin\phi_x\cos\theta_x\cos\phi_L + \cos\phi_y\cos\theta_y\sin\phi_L}{\cos\phi_x\cos\theta_x\cos\phi_L - \sin\phi_y\cos\theta_y\sin\phi_L}\right) \quad (16)$$

$$\theta_B = \theta_L - \cos^{-1}\left(\frac{\cos\theta_L - \cos\phi_L\sin\theta_L\sin\theta_x + \sin\phi_L\sin\theta_L\sin\theta_y}{\sqrt{\begin{array}{r}1+\sin\phi_L\sin(2\theta_L)\sin\theta_y - [\sin\theta_x\\ \cos\phi_L\sin(2\theta_L)+\sin\theta_x\sin\theta_y\\ \sin(2\phi_L)\sin^2\theta_L] + \cos\theta_x\\ \cos\theta_y\sin(2\phi_L)\sin(\phi_x-\phi_y)\sin^2\theta_L\end{array}}}\right) \quad (17)$$

Note the following for (16):

i. ϕ_B is independent on θ_L, which implies that the azimuthal pointing bias does not vary with the look direction polar angle $\theta_L$as long as the vertical leg is perfect (i.e. not mis-oriented).

ii. If $\theta_x=\theta_y$, and $\phi_x=\phi_y$, the azimuthal pointing bias $\phi_B=\pm\phi_x$. The positive sign is holds for $|\theta_x|=|\theta_y|\in\left[0,\frac{\pi}{2}\right]$ while the negative sign holds for$|\theta_x|=|\theta_y|\in\left[\frac{\pi}{2},\pi\right]$. This implies that if orthogonality is maintained between the $\tilde{x}$ and $\tilde{y}$, the azimuthal pointing error is equal to the azimuthal mis-orientation of the two axes.

IV. Further Analyzing The Pointing Bias

The pointing bias has been derived as (16) and (17) in SectionIII. In this section, degenerate cases of one-axis mis-orientations are further discussed.Section IV-A will analyze the case of just mis-oriented x-axiswhile SectionIV-B will analyze that for just mis-oriented y-axis.Finally, SectionIV-C discusses the case of mis-orientation only on the $x0y$ plane.

A. *Case of only mis-oriented x-axis*

In this section, the case of perfect z-axis and y-axis is studied, i.e $\theta_x\in\left[-\frac{\pi}{2},\frac{\pi}{2}\right]$ and $\phi_x\in\left[-\frac{\pi}{2},\frac{\pi}{2}\right]$. Towards this, set $(\theta_y,\phi_y)=(0,0)$ in (16) and (17), and the pointing bias reduce to

$$\phi_{B,x} = \phi_L - \tan^{-1}\left(\frac{\sin\phi_x\cos\theta_x\cos\phi_L+\sin\phi_L}{\cos\phi_x\cos\theta_x\cos\phi_L}\right) \quad (18)$$

$$\theta_{B,x} = \theta_L - \cos^{-1}\left(\frac{\cos\theta_L-\cos\phi_L\sin\theta_L\sin\theta_x}{\sqrt{\begin{array}{r}1-\sin\theta_x\cos\phi_L\sin(2\theta_L)\\ +\cos\theta_x\sin(2\phi_L)\sin(\phi_x)\sin^2\theta_L\end{array}}}\right). \quad (19)$$

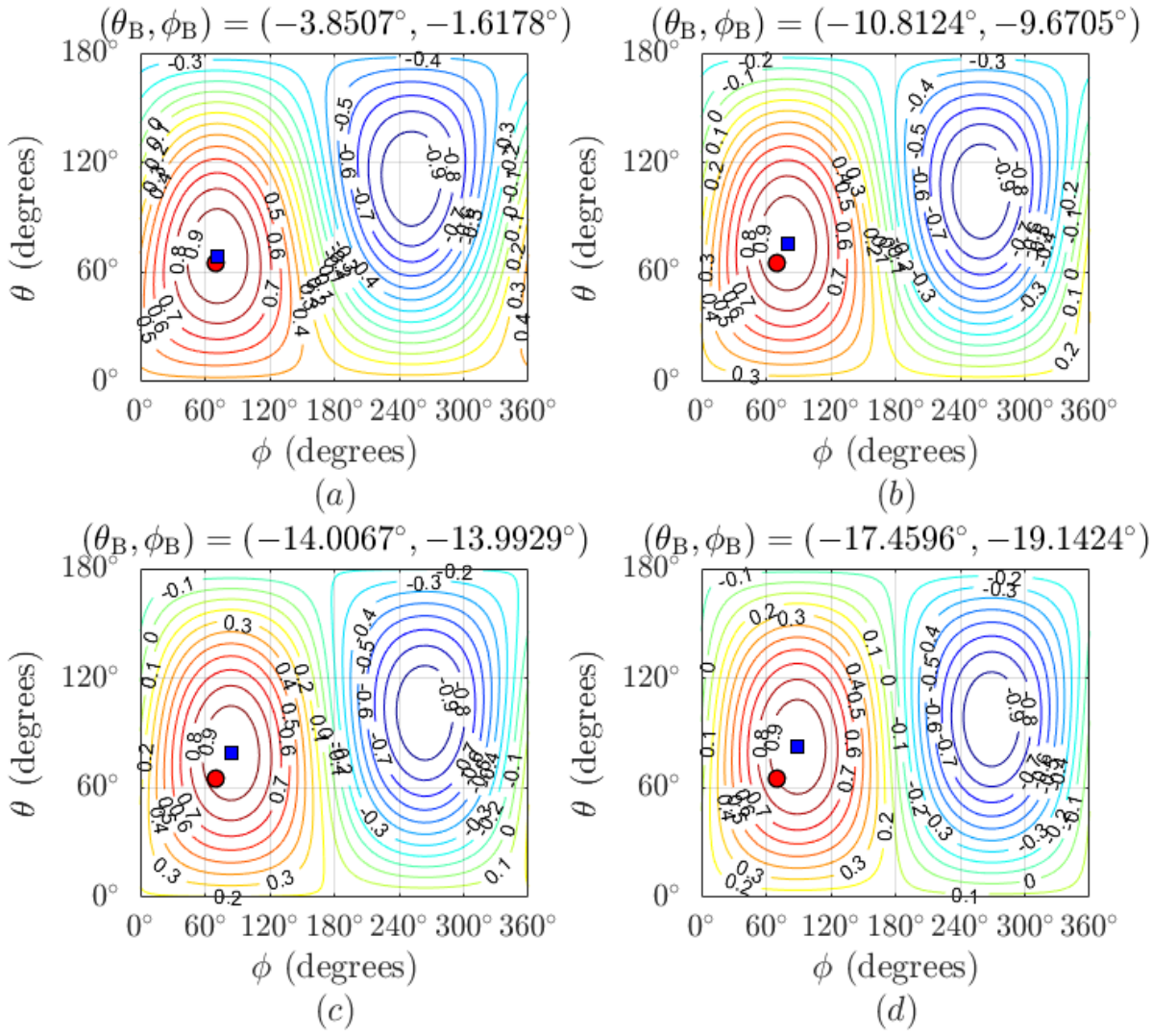

Figure 2. Plots of the beampattern versus the direction of arrival (θ, ϕ) for look direction $(\theta_L, \phi_L) = (65°, 70°)$,$(\theta_y, \phi_y) = (0°, 0°)$, and (a) $(\theta_x, \phi_x) = (10°, 10°)$, (b) $(\theta_x, \phi_x) = (30°, 45°)$, (c) $(\theta_x, \phi_x) = (45°, 60°)$, and (d) $(\theta_x, \phi_x) = (75°, 80°)$. The true peak-direction as blue square and look direction as red circle.

Plots of the beampattern versus the angle of arrival under this condition are contained in Figure 2. The blue square points in the true peak direction while the red circle points in the look direction. Figure 2ashows that the smaller the misorientation the smaller the pointing bias. The pointing bias increases with the misorientation angles as shown across Figure 2a - Figure 2d.

B. *Case of only mis-oriented y-axis*

In this section, the case of perfect z-axis and x-axis is studied, i.e $\theta_y \in \left[-\frac{\pi}{2}, \frac{\pi}{2}\right]$ and $\phi_y \in \left[-\frac{\pi}{2}, \frac{\pi}{2}\right]$. Towards this, set $(\theta_x, \phi_x) = (0, 0)$ in (16) and (17), then the pointing bias reduce to

$$\phi_{B,y} = \phi_L - \tan^{-1}\left(\frac{\cos\phi_y \cos\theta_y \sin\phi_L}{\cos\phi_L - \sin\phi_y \cos\theta_y \sin\phi_L}\right) \quad (20)$$

$$\theta_{B,y} = \theta_L - \cos^{-1}\left(\frac{\cos\theta_L + \sin\phi_L \sin\theta_L \sin\theta_y}{\sqrt{1 + \sin\phi_L \sin(2\theta_L) \sin\theta_y - \cos\theta_y \sin(2\phi_L) \sin\phi_y \sin^2\theta_L}}\right) \quad (21)$$

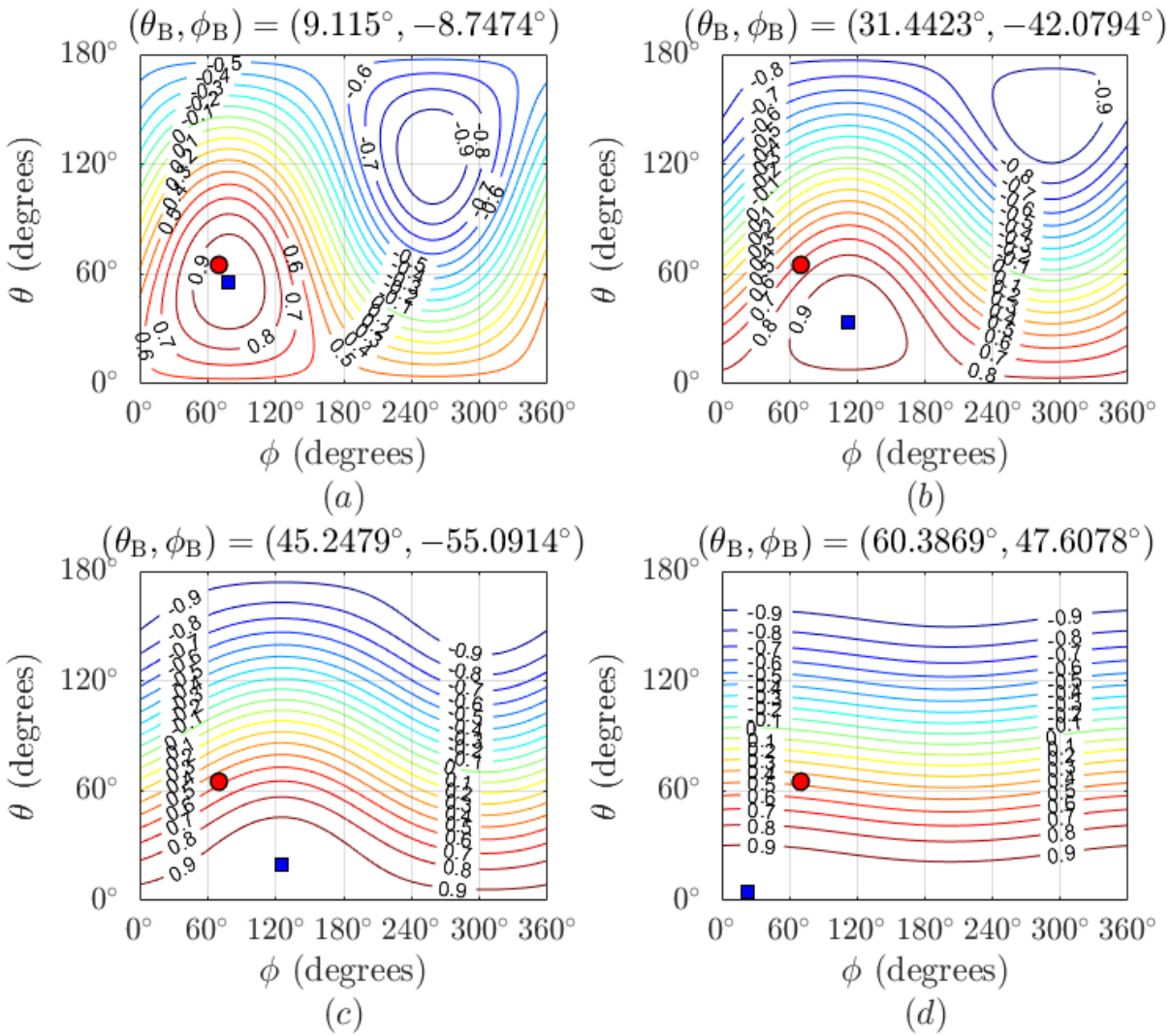

Figure 3: Plots of the beampattern versus the direction of arrival (θ, ϕ) for look direction $(\theta_L, \phi_L) = (65°, 70°)$, $(\theta_x, \phi_x) = (0°, 0°)$, and (a) $(\theta_y, \phi_y) = (10°, 10°)$, (b) $(\theta_y, \phi_y) = (30°, 45°)$, (c) $(\theta_y, \phi_y) = (45°, 60°)$, and (d) $(\theta_y, \phi_y) = (75°, 80°)$. The true peak direction as blue square and look direction as red circle.

Plots of the beampattern versus the angle of arrival under this condition are contained in Figure 3. The blue square points in the true peak direction while the red circle points in the look direction. Figure 3a shows that the smaller the misorientation the smaller the pointing bias. The pointing bias increases with the misorientation angles as shown across Figure 3a-Figure 3d. This trend is similar to what is observed in Section IV-A.

C. *Mis-orientation on the x0y plane*

A more degenerate case of interest is when the mis-orientation occurs on the $x0y$ plane, i.e $\theta_x = \theta_y = 0$. The pointing bias is reduced to

$$\phi_{B,z} = \phi_L - \tan^{-1}\left(\frac{\sin\phi_x \cos\phi_L + \cos\phi_y \sin\phi_L}{\cos\phi_x \cos\phi_L - \sin\phi_y \sin\phi_L}\right) \quad (22)$$

$$\theta_{B,z} = \theta_L - \cos^{-1}\left(\frac{\cos\theta_L}{\sqrt{1 + \sin(2\phi_L)\sin(\phi_x - \phi_y)\sin^2\theta_L}}\right) \quad (23)$$

The expressions (22) and (23) describe the pointing error for a case in which the mis-orientation only affects the horizontal legs on the x0y plane. If the two horizontal axes experience similar azimuthal mis-orientation, i.e.$\phi_x = \phi_y$, (22) and (23) are further reduced to

$$\phi_{B,z} = -\phi_x \quad (24)$$

$$\theta_{B,z} = 0. \quad (25)$$

Therefore, if orthogonality is maintained between the horizontal axes, the polar angle pointing bias is zero.

V. Directivity Of The Non-Orthogonal Tri-Axial Velocity Sensor

In this section, the directivity of the non-perpendicular tri-axial velocity sensor is analyzed to study how the non-orthogonality affects the directivity of the non-perpendicular tri-axial velocity sensor in the look direction.

Directivity is defined in[11]for the spherical noise field

$$D := \frac{B(\theta_L, \phi_L)^2}{\frac{1}{4\pi}\int_{\phi=0}^{2\pi}\int_{\theta=0}^{\pi} B(\theta,\phi)^2 \sin\theta \, d\theta \, d\phi}, \quad (26)$$

where $B(\theta, \phi)$ is the beampattern andother variables as previously defined. The denominator of (26) evaluates to 1/3. Therefore, the directivity equals

$$D = 3B^2(\theta_L, \phi_L). \quad (27)$$

$B|_{(\theta,\phi)=(\theta_{\text{peak}},\phi_{\text{peak}})} \geq B|_{(\theta,\phi)=(\theta_L,\phi_L)}$,hence$B|_{(\theta,\phi)=(\theta_L,\phi_L)} \leq 1$. Therefore, the directivity of the non-perpendicular tri-axial velocity sensor is less than or equal 3. The directivity of the perfect tri-axial velocity sensor is equal to 3 [11].

VI. Conclusion

This paper analyzed the pointing error in the spatial matched-filter beampattern of a tri-axial velocity sensorsubject to mutual non-orthogonality. The case of perfect vertical axis was studied with degenerate cases of this further analyzed. The effect of this non-perpendicularity on the directivity was analyzed. When the axes are not mutually orthogonal, the shape ofthe beampattern remains unchanged but the effective lookdirection will mis-point by an offset which dependson the nominal look direction and how much the axesdeviate from the nominal Cartesian axes. In terms of directivity, the directivity of the imperfect tri-axial velocity sensor was shown less than or equal 3, i.e. value for a perfect tri-axial velocity sensor.

References

[1] A. Nehorai and E. Paldi, "Acoustic vector-sensor array processing," *IEEE Trans. Signal Process.*, vol. 42, no. 9, pp. 2481–2491, 1994.

[2] Y. I. Wu, K. T. Wong, and S.-K. Lau, "The acoustic vector-sensor's near-field array-manifold," *IEEE Trans. Signal Process.*, vol. 58, no. 7, pp. 3946–3951, 2010.

[3] Y. I. Wu, S.-K. Lau, and K. T. Wong, "Near-field/far-field array manifold of an acoustic vector-sensor near a reflecting boundary," *J. Acoust. Soc. Am.*, vol. 139, no. 6, pp. 3159–3176, 2016.

[4] P. K. Tam and K. T. Wong, "Cram\'{e}r-Rao bounds for direction finding by an acoustic vector-sensor under non-ideal gain-phase responses, non-collocation, or non-orthogonal orientation," *IEEE Sens. J.*, vol. 9, no. 8, pp. 969–982, 2009.

[5] Y. I. Wu and K. T. Wong, "Acoustic near-field source localization by two passive anchor nodes," *IEEE Trans. Aerosp. Electron. Syst.*, vol. 48, no. 1, pp. 159–169, 2012.

[6] M. K. Awad and K. T. Wong, "Recursive least-squares source-tracking using one acoustic vector-sensor," *IEEE Trans. Aerosp. Electron. Syst.*, vol. 48, no. 4, pp. 3073–3083, 2012.

[7] B. D. Van Veen and K. M. Buckley, "Beamforming: a versatile approach to spatial filtering," *IEEE Acoust. Speech Signal Process. Mag.*, vol. 5, no. 2, pp. 4–24, 1988.

[8] K. T. Wong and H. Chi, "Beam patterns of an underwater acoustic vector hydrophone located away from any reflecting boundary," *IEEE J. Ocean. Eng.*, vol. 27, no. 3, pp. 628–637, 2002.

[9] T.-C. Lin, K. T. Wong, M. O. Cordel, and J. P. Ilao, "Beamforming pointing error of a triaxial velocity sensor under gain uncertainties," *J. Acoust. Soc. Am.*, vol. 140, no. 3, pp. 1675–1685, 2016.

[10] C. H. Lee, H. R. L. Lee, K. T. Wong, and M. Razo, "The spatial-matched-filter beam pattern of a biaxial non-orthogonal velocity sensor," *J. Sound Vib.*, vol. 367, pp. 250–255, 2016.

[11] Y. Huang and J. Benesty, *Audio Signal Processing for Next-Generation Multimedia Communication Systems*. New York, U.S.A: Kluwer Academic Publishers, 2004.